

Intramolecular Hydrogen Bonding Plays a Crucial Role in the Photophysics and Photochemistry of the GFP Chromophore

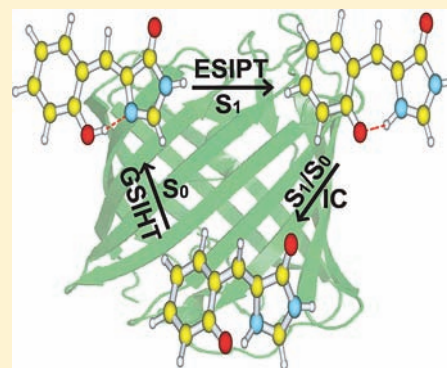
Ganglong Cui,[†] Zhenggang Lan,[‡] and Walter Thiel^{*,†}

[†]Max-Planck-Institut für Kohlenforschung, Kaiser-Wilhelm-Platz 1, 45470 Mülheim an der Ruhr, Germany

[‡]Qingdao Institute of Bioenergy and Bioprocess Technology, Chinese Academy of Sciences, Qingdao 266101, P.R. China

S Supporting Information

ABSTRACT: In commonly studied GFP chromophore analogues such as 4-(4-hydroxybenzylidene)-1,2-dimethyl-1H-imidazol-5(4H)-one (PHBDI), the dominant photoinduced processes are cis–trans isomerization and subsequent $S_1 \rightarrow S_0$ decay via a conical intersection characterized by a highly twisted double bond. The recently synthesized 2-hydroxy-substituted isomer (OHBDI) shows an entirely different photochemical behavior experimentally, since it mainly undergoes ultrafast intramolecular excited-state proton transfer, followed by $S_1 \rightarrow S_0$ decay and ground-state reverse hydrogen transfer. We have chosen 4-(2-hydroxybenzylidene)-1H-imidazol-5(4H)-one (OHBI) to model the gas-phase photodynamics of such 2-hydroxy-substituted chromophores. We first use various electronic structure methods (DFT, TDDFT, CC2, DFT/MRCI, OM2/MRCI) to explore the S_0 and S_1 potential energy surfaces of OHBI and to locate the relevant minima, transition state, and minimum-energy conical intersection. These static calculations suggest the following decay mechanism: upon photoexcitation to the S_1 state, an ultrafast adiabatic charge-transfer induced excited-state intramolecular proton transfer (ESIPT) occurs that leads to the S_1 minimum-energy structure. Nearby, there is a S_1/S_0 minimum-energy conical intersection that allows for an efficient nonadiabatic $S_1 \rightarrow S_0$ internal conversion, which is followed by a fast ground-state reverse hydrogen transfer (GSHT). This mechanism is verified by semiempirical OM2/MRCI surface-hopping dynamics simulations, in which the successive ESIPT–GSHT processes are observed, but without cis–trans isomerization (which is a minor path experimentally with less than 5% yield). These gas-phase simulations of OHBI give an estimated first-order decay time of 476 fs for the S_1 state, which is larger but of the same order as the experimental values measured for OHBDI in solution: 270 fs in CH_3CN and 230 fs in CH_2Cl_2 . The differences between the photoinduced processes of the 2- and 4-hydroxy-substituted chromophores are attributed to the presence or absence of intramolecular hydrogen bonding between the two rings.



INTRODUCTION

Green fluorescence proteins (GFP) have been the subject of much interest because of their ubiquitous applications in molecular biology. They can be used as fluorescent marker proteins in living organisms—a revolutionary advance in bioimaging.^{1–10} Numerous experimental and theoretical studies have been undertaken to understand the photophysics and photochemistry of the GFP chromophore upon photoexcitation. These include characterization of absorption and emission bands in optical spectra as well as excited-state dynamics simulations in various environments, for example in vacuum, in solution, and in proteins.^{10–23}

The GFP chromophore is anchored on proteins covalently or via a hydrogen-bonding network (see Figure 1). It is formed through an autocatalytic reaction after expression and folding. To better understand the intrinsic photophysical properties of the GFP chromophore independently from its protein environment, many spectroscopic and computational studies have targeted synthetic analogues of the GFP chromophore with a 4-hydroxybenzylidene-imidazolone motif.^{10–52} One of the most often studied synthetic models is 4-(4-hydroxybenzylidene)-1,2-dimethyl-1H-imidazol-5(4H)-one (PHBDI), see Figure 2. Also frequently used is a truncated model, 4-(4-hydroxybenzylidene)-1H-imidazol-5(4H)-one (PHBI), which preserves the conjugated system (Figure 2). PHBI differs from PHBDI in that methyl groups positioned at the linkage to proteins are replaced by hydrogen atoms.

These two model chromophores (PHBDI and PHBI) exhibit analogous photophysical and photochemical mechanisms because they share the same motif, 4-hydroxybenzylidene-imidazolone. Their absorption and emission spectra have been extensively studied both experimentally and theoretically,^{3,4,18–20,22,49,50,53} but there has been less work on the $S_1(^1\pi\pi^*)$ excited-state dynamics. Two main decay mechanisms have been proposed for PHBDI and PHBI. The first one involves cis–trans isomerization of the central double bond, as illustrated in Figure 3. In the experimental studies, this is considered to be a major or even predominant decay channel in vacuum and solution after the bright $S_1(^1\pi\pi^*)$ singlet state is

Received: September 15, 2011
Published: December 15, 2011

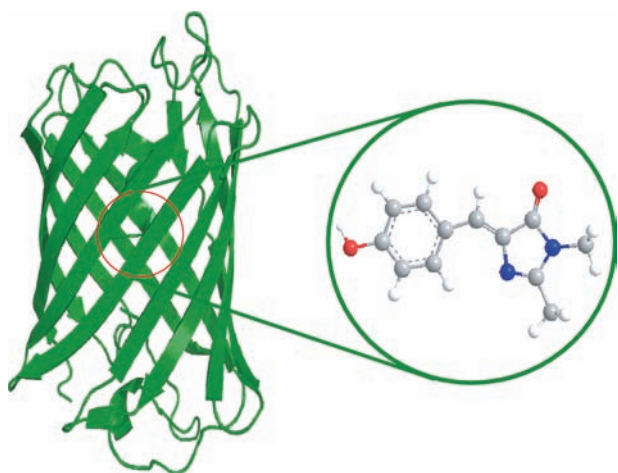


Figure 1. Schematic drawing of green fluorescence protein and its core chromophore, *p*-hydroxybenzylidene-imidazolone.

populated.^{21,50,53} In this mechanism, the bridging double bond twists, leading to a twisted/perpendicular $S_1(^1\pi\pi^*)$ intermediate, with a nearby $S_1(^1\pi\pi^*)/S_0$ minimum-energy conical intersection that funnels electronic population to the S_0 state. Quantum chemical calculations and dynamics simulations have supported this decay mechanism.^{15–17,39,41,42,44,45,48} Early work by Martin et al. and Altoe et al. addressed the key $S_1(^1\pi\pi^*)/S_0$ conical intersection and the $S_1(^1\pi\pi^*)$ excited-state properties using the complete active space self-consistent field (CASSCF) method.^{16,17} Olsen and Smith computed stationary points on the S_0 and $S_1(^1\pi\pi^*)$ surfaces and located the $S_1(^1\pi\pi^*)/S_0$ minimum-energy conical intersection at the CASSCF level.⁴¹ More recently, Olsen et al. investigated the effect of protonation on the excited-state isomerization of isolated PHBI by CASSCF ab initio molecular dynamics: they found that both neutral and anionic forms of PHBI undergo fast cis–trans isomerizations.⁴⁸ Martinez et al. applied multiple-spawning nonadiabatic wavepacket dynamics to study photo-induced processes of PHBDI and PHBI in vacuum, in solution, and in proteins;^{13,15,42} they observed cis–trans isomerization in vacuum both at the semiempirical and ab initio levels, and examined the influence of solvent and protein environments within a quantum mechanics/molecular mechanics (QM/MM) framework. One should note in this context that the cis–trans double-bond isomerization mechanism is quite general and also

operates in chromophores of the red fluorescence protein, the photoactive yellow protein, and others.^{27,39,52,54–59} In spite of the preponderance of this mechanism in photochemistry, it is conceivable that this decay channel could be prohibited in proteins because of the structured hydrogen-bonding environment of the core moiety. An alternative decay mechanism (Figure 3) involves excited-state proton transfer via a hydrogen-bonding network formed between the chromophore, active-site residues, and water molecules.^{3,4,10,18,20,22}

Recent research on GFP chromophores has addressed 4-(2-hydroxybenzylidene)-1,2-dimethyl-1H-imidazol-5(4H)-one (OHBDI) and its derivatives (Figure 2).^{60–62} Chen et al. designed and synthesized this modified GFP chromophore in 2007.⁶⁰ It contains an intramolecular hydrogen bond, which links the two rings of the chromophore and thus allows for an excited-state intramolecular proton transfer (ESIPT) without assistance from the solvent or other molecules. Recently, Chou and co-workers comprehensively studied the overall proton transfer reaction cycle in OHBDI by using time-resolved ultraviolet-vis and mid-infrared spectroscopy, steady-state and pump–probe transient absorption, and two-step laser-induced fluorescence.⁶¹ They observed that the cis–trans isomerization yield is less than 5% and that more than 95% of the excited-state tautomers of OHBDI decay to the ground state via an ESIPT process that is completed in less than 25 fs. This experimental work thus indicates a dominant ESIPT mechanism in the excited-state dynamics of OHBDI followed by a reverse hydrogen transfer in the ground state. In this mechanistic scenario, there are a number of open questions that cannot be answered solely by experimental means and that call for a detailed theoretical investigation. For example: Why is the ESIPT process ultrafast in OHBDI? When and how does the $S_1 \rightarrow S_0$ internal conversion occur? What is the structure of the S_1/S_0 conical intersection that is responsible for this internal conversion? What is the origin of the fast (fs) and slow (ps) decay components? Why is the quantum yield for cis–trans isomerization of OHBI so low (less than 5%)? Furthermore, compared with that of PHBI and PHBDI, the photoinduced dynamics of OHBDI is remarkably different, and it is clearly worthwhile to study the cause of these differences and thus improve our understanding of the intrinsic photophysical properties of GFP chromophores.^{13,15,39,41,42,48} This again requires theoretical calculations.

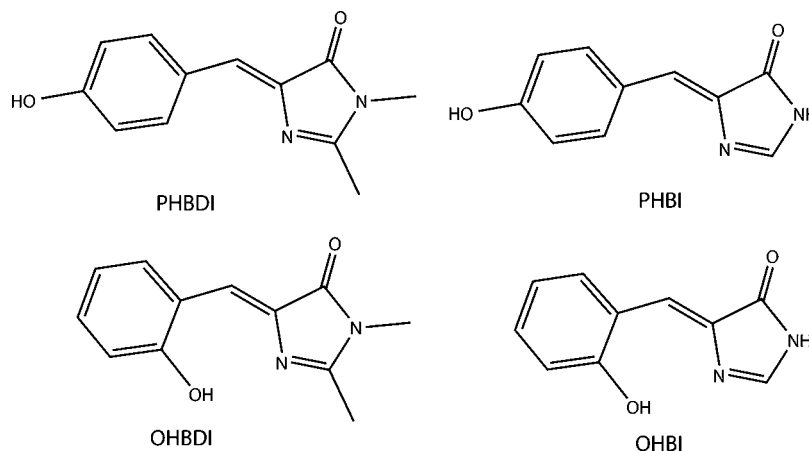


Figure 2. Model chromophores related to green fluorescence proteins.

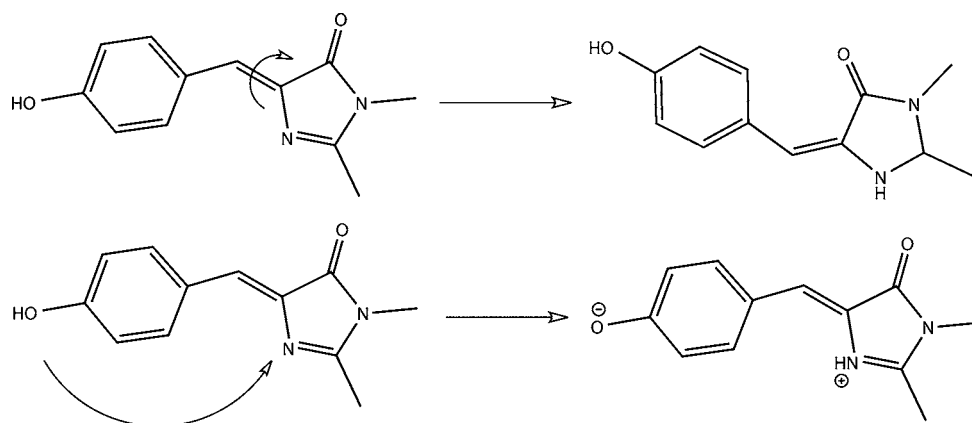


Figure 3. Two possible decay mechanisms (top: cis–trans isomerization; bottom: excited-state proton transfer mediated by nearby water molecules or residues) in PHBDI and PHBI models of the GFP core chromophore.

To the best of our knowledge, there are no published computational studies that address the photodynamics of OHBDI. In this work, we investigate a truncated model, 4-(2-hydroxybenzylidene)-1H-imidazol-5(4H)-one (OHBI), which retains the conjugated system of OHBDI that is essential for the electronic excitation. This simplification of replacing two methyl substituents by hydrogen saves computational effort and has been employed in an analogous manner in previous work on the 4-hydroxy-substituted systems that modeled PHBI instead of PHBDI.^{15,42} We have performed static *ab initio* and density functional calculations to characterize the relevant potential energy surfaces of OHBI. The resulting mechanistic proposal for the photochemistry and the excited-state decay of OHBI has been checked and verified by OM2/MRCI nonadiabatic dynamics simulations.

■ COMPUTATIONAL DETAILS

Ab Initio and Density Functional Methods. The stationary points on the S_0 and S_1 potential energy surfaces of OHBI were optimized using density functional theory (DFT, S_0), time-dependent DFT (TDDFT, S_1), and coupled cluster theory (CC2, S_0 and S_1).^{63–67} Vertical excitation energies at the ground-state geometries were computed using TDDFT with different functionals (B3LYP, CAM-B3LYP, ω B97XD, M06-2X), DFT-based multireference configuration interaction (DFT/MRCI), and CC2.^{64–66,68–73} To be consistent with the original parametrization, the DFT/MRCI work employed the B3LYP functional.^{70,74} The following basis sets were used: 6-31+G* for optimization with DFT and TDDFT,⁷⁵ aug-cc-pVDZ for single-point TDDFT,⁷⁶ and TZVP for CC2 and DFT/MRCI.⁷⁷ The DFT and TDDFT calculations were carried out using the GAUSSIAN09 package,⁷⁸ whereas the CC2 and DFT/MRCI calculations were done with TURBOMOLE6.3 and TURBOMOLE.7, respectively.⁷⁹

Semiempirical Methods. All semiempirical calculations were performed using the OM2/MRCI method^{80–83} as implemented in the MNDO99 program.⁸⁴ The restricted open-shell Hartree–Fock formalism was applied in the self-consistent field (SCF) treatment (i.e., the orbitals were optimized for the leading configuration of the S_1 state with two singly occupied π orbitals). The active space in the MRCI calculations included 12 electrons in 12 orbitals: in terms of the SCF configuration, it comprised the five highest doubly occupied π orbitals, the two singly occupied π orbitals, and all five unoccupied π^* orbitals; n orbitals were not included since the S_1 state is of $\pi \rightarrow \pi^*$ type. For the MRCI treatment, three configuration state functions were chosen as references, namely the SCF configuration and the two closed-shell configurations derived therefrom (i.e., all singlet configurations that can be generated from the HOMO and LUMO of the closed-shell ground state). The MRCI wave function was built by allowing all single and double excitations from these three

references. During OM2/MRCI geometry optimizations and dynamics simulations, all required gradients and nonadiabatic coupling elements were computed analytically,⁸² and to maintain a uniform active space the character of the orbitals was tracked automatically using a previously described procedure.⁸⁵ Briefly, in this procedure, local π populations are computed for each orbital with respect to the local plane at a given π center, and their sum must be greater than a threshold (here: 0.3) for the orbital to qualify as π orbital.

The S_0 and S_1 minimum-energy structures and the S_1/S_0 minimum-energy conical intersection were optimized at the OM2/MRCI level. Vertical excitation energies were computed by OM2/MRCI at the optimized ground-state geometries.

Photoinduced nonadiabatic dynamics was followed by OM2/MRCI trajectory surface hopping.^{86,87} The initial atomic coordinates and velocities were randomly selected from 5 ps trajectories of ground-state molecular dynamics. The number of excited-state dynamics runs for each chosen snapshot was chosen according to the computed $S_0 \rightarrow S_1$ transition probabilities. A total of 400 surface-hopping trajectories were run and evaluated in the present nonadiabatic OM2/MRCI simulations, with all relevant energies, gradients, and nonadiabatic coupling vectors being computed on-the-fly as needed. The fewest-switches criterion was applied to decide whether to hop.^{86,88–90} The time step was chosen to be 0.1 fs for the nuclear motion and 0.0005 fs for the electronic propagation. Further technical details are given in previous publications.^{91–95}

■ RESULTS AND DISCUSSION

S_0 Equilibrium Structure and Vertical Excitation Energy. The most stable S_0 equilibrium structure of OHBI (S0-MIN) has an intramolecular hydrogen bond between its two rings, which are therefore in a *cis* arrangement (Figure 4), consistent with experiment.⁶¹ All computational methods applied predict that S0-MIN is planar (C_s symmetry). The computed geometric parameters are collected in Table 1.

Since this work focuses on decay pathways of the $S_1(1\pi\pi^*)$ state of OHBI, we only discuss the vertical excitation energy to this lowest excited singlet state (Table 2). It is obvious that the CC2, OM2/MRCI, and most of TDDFT results are quite close to each other, which provides support to our choice of active space and reference configurations in the OM2/MRCI calculations. The $S_0 \rightarrow S_1$ transition is essentially a one-electron HOMO–LUMO excitation that is accompanied by a partial charge transfer from the six-membered to the five-membered ring, as can be seen from the schematic HOMO and LUMO plots with an isosurface value of 0.05 in Figure 5. Given this situation, it is not surprising that TD-B3LYP (CAM-B3LYP) gives the lowest (highest) excitation energy (71.0 vs 79.1 kcal/

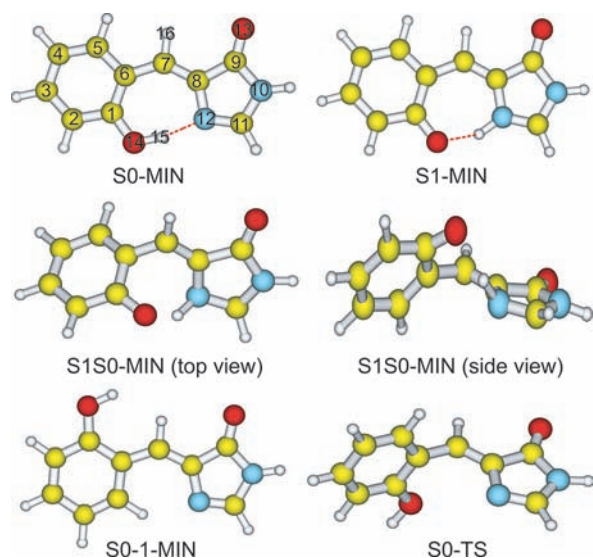


Figure 4. Schematic plots of the OHBI structures optimized in this work. See Table 1 for the numerical values of key geometric parameters.

mol): for charge-transfer excited states, TD-B3LYP is known to underestimate excitation energies, whereas range-separated exchange-correlation functionals such as CAM-B3LYP usually perform better. The modern M06-2X functional and the coupled cluster CC2 method also yield rather high values (78.5 and 77.2 kcal/mol, respectively). The OM2/MRCI result of 75.5 kcal/mol for gas-phase OHBI is fortuitously close to the vertical excitation energies measured for OHBDI in solution: 74.3 kcal/mol in C_6H_{12} , 75.2 kcal/mol in H_2O at pH = 7.⁶⁰

The vertical $S_0 \rightarrow S_1$ transition leads to a significant increase of the dipole moment of OHBI calculated at the S0-MIN geometry (CC2/TZVP from 2.15 to 3.75 D; OM2/MRCI from 1.81 to 4.30 D), which reflects the charge-transfer character of the S_1 state.

$S_1(^1\pi\pi^*)$ Equilibrium Structure and Vertical Emission Energy. At the CC2/TZVP and OM2/MRCI levels, we have optimized the structure of the S_1 state (S1-MIN, Figure 4). While it also has C_s symmetry, it is qualitatively different from S0-MIN because the H15 atom that is attached to the O14 atom in the S_0 state, is bonded to the N12 atom in the S_1 state. The other structural changes between S0-MIN and S1-MIN are gradual and can be assessed from Table 1. The potential energy of S1-MIN relative to S0-MIN is predicted to be 63.0, 63.1, and 58.3 kcal/mol at the CC2, TDDFT, and OM2/MRCI levels, respectively.

The S1-MIN structure of OHBI is also qualitatively different from the S_1 equilibrium structures of PHBI and PHBDI, which are nonplanar and have the two rings nearly perpendicular to each other.^{15,42,48} The planarity of S1-MIN in OHBI is due to the intramolecular hydrogen bonding involving the O14, H15, and N12 atoms, which is not present in PHBDI and PHBI.¹⁵

At the S_1 minimum-energy structure, S1-MIN, the $S_1 \rightarrow S_0$ emission energy of OHBI in the gas phase is calculated to be 1.97 eV (629 nm) at the CC2/TZVP level and 1.95 eV (636 nm) at the OM2/MRCI level, in reasonable agreement with the experimentally measured values of 2.05 eV (605 nm) and 2.06 eV (602 nm) for OHBDI in cyclohexane and acetonitrile solution, respectively.⁶¹ The computed Stokes shifts for OHBI (CC2/TZVP from 370 to 629 nm; OM2/MRCI from 379 to 636 nm) also reproduce the experimental values for OHBDI well (from 385 to 605 nm in cyclohexane and from 383 to 602 nm in acetonitrile).⁶¹ The radiative lifetime for vertical emission at S1-MIN is predicted to be 18 ns (OM2/MRCI).

$S_1(^1\pi\pi^*)/S_0$ Minimum-Energy Conical Intersection. The $S_1(^1\pi\pi^*)/S_0$ minimum-energy conical intersection has been optimized at the OM2/MRCI level (S1S0-MIN, Figure 4). The hydrogen-bonding moiety (O14...H15–N12) remains largely intact in S1S0-MIN, as indicated by the corresponding distances (Table 1) and the fact that this part of the molecule remains close to planar (dihedral angle of 12°), thus maintaining some link between the two rings of the OHBI molecule. By contrast, in PHBI where the intramolecular hydrogen bond is missing, the $S_1(^1\pi\pi^*)/S_0$ minimum-energy conical intersection has the two rings nearly perpendicular to each other.^{13,15,42}

The potential energy of S1S0-MIN relative to S0-MIN is computed to be 63.8 kcal/mol at the OM2/MRCI level. Hence, S1S0-MIN lies 5.5 kcal/mol above S1-MIN, but 11.7 kcal/mol below the Franck–Condon point that is reached initially upon vertical photoexcitation to the S_1 state. Access to this minimum-energy conical intersection should thus be facile, because the small energy barrier of 5.5 kcal/mol from S1-MIN should easily be overcome by the energy gained during the relaxation process from the Franck–Condon point to S1-MIN.

Considering that the $S_1(^1\pi\pi^*)$ equilibrium structure and the $S_1(^1\pi\pi^*)/S_0$ minimum-energy conical intersection in OHBI are very different from those in PHBI and PHBDI, we expect that the $S_1(^1\pi\pi^*)$ decay processes of OHBI and PHBI will also be rather different. This is borne out by the OM2/MRCI trajectory surface hopping dynamics simulations that are described below.

Intramolecular Excited-State Charge-Induced Proton Transfer. As already explained, the vertical $S_0 \rightarrow S_1(^1\pi\pi^*)$

Table 1. Key Bond Lengths (Å) and Dihedral Angles (deg) in the Optimized Structures of OHBI

	C1O14	O14H15	N12H15	C1C6C7C8	C6C7C8N12	H15N12C8C9
S0-MIN ^a	1.329	1.020	1.562	0.0	0.0	180.0
S0-MIN ^b	1.343	1.003	1.629	0.0	0.0	180.0
S0-MIN ^c	1.341	1.000	1.671	0.0	0.0	180.0
S0-1-MIN ^c	1.365	0.969	4.973	180.0	0.0	180.0
S0-TS ^c	1.371	0.970	4.477	−84.6	0.4	−133.8
S1-MIN ^a	1.266	1.464	1.067	0.0	0.0	180.0
S1-MIN ^b	1.320	1.509	1.079	0.0	0.0	180.0
S1-MIN ^d	1.287	1.571	1.068	0.0	0.0	180.0
S1S0-MIN ^a	1.264	1.651	1.068	60.7	−11.7	136.1

^aOM2/MRCI. ^bCC2/TZVP. ^cDFT(B3LYP)/6-31+G*. ^dTDDFT(B3LYP)/6-31+G*.

Table 2. Vertical Excitation Energies to the S_1 State of OHBI, in kcal/mol (first row) and in eV (second row)

CC2 ^a	DFT/MRCI ^a	OM2/MRCI	B3LYP ^b	CAM-B3LYP ^b	ω B97XD ^b	M06-2X ^b	EXP ^c	EXP ^d
77.3	73.4	75.5	71.0	78.6	79.1	78.5	74.3	75.2
3.35	3.18	3.27	3.08	3.41	3.43	3.40	3.22	3.26

^aCC2/TZVP geometry. ^bB3LYP/6-31+G* geometry. ^cExperimental value in cyclohexane. ^dExperimental value in water at pH = 7.

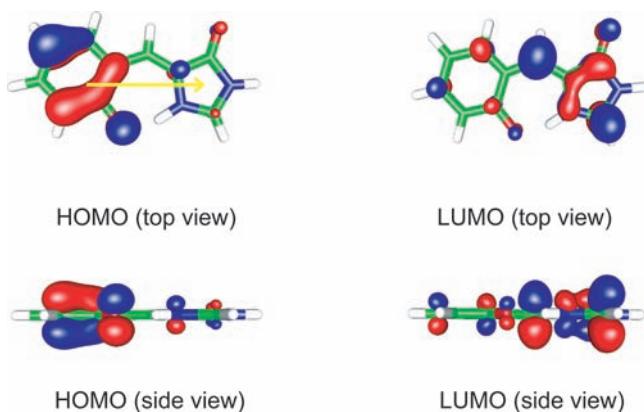


Figure 5. Schematic plots of molecular orbitals: HOMO and LUMO of OHBI (CC2/TZVP). The computed transition dipole moment vector (yellow arrow) points from the phenyl to the imidazole ring.

transition in the Franck–Condon region corresponds essentially to the excitation of an electron from HOMO to LUMO, which are mostly located in different parts of the molecule, i.e., in the six- and five-membered ring, respectively (see Figure 5). Thus, the $S_0 \rightarrow S_1(^1\pi\pi^*)$ transition is accompanied by a transfer of negative charge from the phenyl group to the five-membered ring, which will facilitate or even trigger the subsequent transfer of a proton in the same direction.

This transfer occurs spontaneously during geometry optimization of the S_1 state, both at the CC2 and OM2/MRCI levels: when starting the S_1 optimization from the S_0 equilibrium structure (S_0 -MIN), the H15 proton rapidly moves downhill toward the N12 atom and ends up at the $S_1(^1\pi\pi^*)$ equilibrium structure, S_1 -MIN, where it is bonded to the N12 atom. An analogous behavior is seen in the OM2/MRCI surface-hopping dynamics simulations: the H15 proton originally attached to the O14 atom (see Figure 4) moves in an ultrafast process to the N12 atom. In all trajectories, the excited-state proton transfer is completed within tens of femtoseconds, similar to the experimentally observed time scale of less than 25 fs for OHBDI.⁶¹

The proton transfer lowers the computed dipole moment of the S_1 state of OHBI appreciably: going from the Franck–Condon geometry (S_0 -MIN) to the excited-state minimum (S_1 -MIN) leads to reductions from 3.75 to 2.30 D for CC2/TZVP and from 4.30 to 1.95 D for OM2/MRCI.

Experimentally, two oscillation frequencies at 115 and 236 cm^{-1} have been identified in the time-resolved fluorescence signal of the tautomer emission, implying that the ESIP process is fast enough to be impulsive with regard to these vibrations, which have been attributed to in-plane skeletal modes involving the hydrogen-bonding moiety on the basis of quantum chemical calculations (CIS/6-31G*).⁶¹ Our present results support this interpretation: at the OM2/MRCI level, the two lowest in-plane modes of the S_1 state of OHBI are found at 159 and 261 cm^{-1} and involve deformations of the intramolecular hydrogen bond.

Internal Conversion $S_1 \rightarrow S_0$. After completing the ultrafast ESIP process, the molecule will move around the $S_1(^1\pi\pi^*)$ minimum-energy structure (S_1 -MIN). The $S_1(^1\pi\pi^*)/S_0$ minimum-energy conical intersection (S_1S_0 -MIN) is geometrically close to S_1 -MIN (see Figure 4): in both structures, H15 is attached to N12, and the intramolecular hydrogen bond is present (albeit distorted in S_1S_0 -MIN); unlike S_1 -MIN, however, S_1S_0 -MIN is nonplanar and differs from S_1 -MIN mainly with regard to several torsional parameters (see Table 1). The proximity, both in terms of structure and energetics (see above), makes S_1S_0 -MIN easily accessible from S_1 -MIN, so that the $S_1(^1\pi\pi^*)$ electronic population can be funneled to the ground state efficiently, resulting in an ultrafast internal conversion to the S_0 state via S_1S_0 -MIN.

In the OM2/MRCI nonadiabatic simulations, the main radiationless transition does indeed take place near the $S_1(^1\pi\pi^*)/S_0$ minimum-energy conical intersection, S_1S_0 -MIN. We have analyzed the structural characteristics of the $S_1 \rightarrow S_0$ hopping points from all trajectories. The distributions of some key geometric parameters are plotted in Figures 6 and 7. The

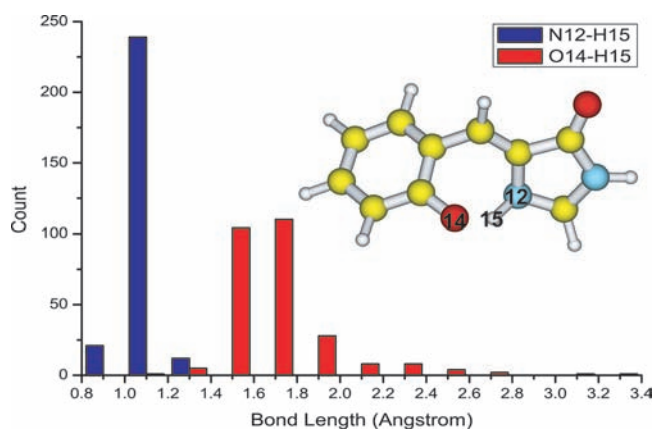


Figure 6. Distributions of the N12–H15 and O14–H15 distances at the $S_1 \rightarrow S_0$ hopping points. The abscissa and ordinate represent the distances (Å) and the number of trajectories, respectively.

former shows that the N12–H15 bond length is typically around 1.0 Å at all hopping points; while the O14–H15 distance varies mostly between 1.6 and 1.8 Å, with some values around 2.0 Å. The latter figure illustrates distributions of some key angles and dihedral angles at the hopping points. The C1–C6–C7–C8 and C6–C7–C8–C12 dihedral angles represent rotations around the C6–C7 and C7–C8 bonds, while the H16–C7–C8–N12 dihedral angle describes pyramidalization at the C7 atom. Figure 7 clearly shows that at all hopping points in the current simulations, the C6–C7–C8–C12 and H16–C7–C8–N12 moieties are nearly planar, with dihedral angles around 165° and 20°, respectively; the C1–C6–C7–C8 dihedral angle oscillates around 60°. These distributions are consistent with the OM2/MRCI optimized structure of the $S_1(^1\pi\pi^*)/S_0$ minimum-energy conical intersection, S_1S_0 -MIN

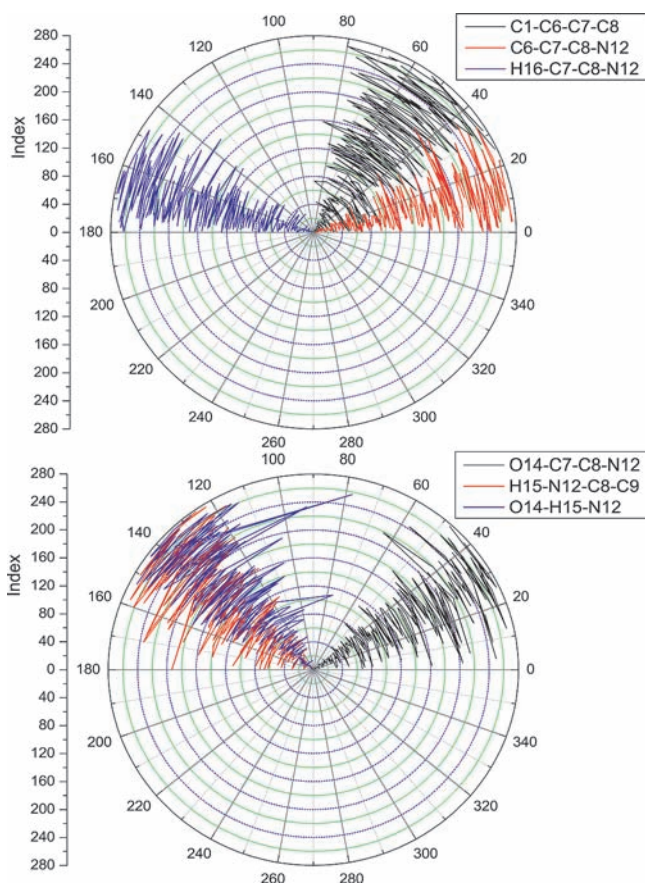


Figure 7. Distributions of key angles and dihedral angles at the $S_1 \rightarrow S_0$ hopping points. The ordinate represents the index associated with each trajectory. The C1–C6–C7–C8 and C6–C7–C8–C12 dihedral angles refer to rotations around the C6–C7 and C7–C8 bonds; the H16–C7–C8–N12 and H15–N12–C8–C9 dihedral angles describe pyramidalizations at the C7 and N2 atoms; the O14–C7–C8–N12 dihedral angle measures the degree of cis–trans isomerization; the O14–H15–N12 angle characterizes the corresponding hydrogen bond.

(see Table 1). Furthermore, at the hopping points, there is no evidence for cis–trans isomerization since the O14–C7–C8–N12 dihedral angle always has rather low values of about 30° . There is some pyramidalization at the N12 atom, as indicated by H15–N12–C8–C9 dihedral angles of about 150° (Figure 7). Finally, the O14–H15–N12 angles of about 140° show that the intramolecular hydrogen bond is no longer fully linear at the hopping points, see Figure 7.

The decay time can be determined from the time-dependent populations of the $S_1(^1\pi\pi^*)$ and S_0 states, which become equal after 330 fs in the OM2/MRCI surface-hopping dynamics simulations (see crossing point in panel a of Figure 8). In terms of unimolecular rate theory, the S_1 state population is given by

$$P(t) = P_0 \exp(-kt) \quad (1)$$

where k is the first-order rate constant and P_0 is the initial S_1 state population. The $S_1(^1\pi\pi^*) \rightarrow S_0$ decay time $\tau_1 = (1/k) = 330 \text{ fs} / \ln 2$ for gas-phase OHBI amounts to 476 fs at the OM2/MRCI level, which is of the same order as the experimentally measured values for OHBDI in solution, i.e., 270 fs in CH_3CN and 230 fs in CH_2Cl_2 .⁶¹

Transformations in the S_0 State. The internal conversion generates the ground state in a fairly distorted geometry close to S1S0-MIN. The S_0 state is an open-shell diradical at such a geometry, which is rather unstable and will rearrange by hydrogen transfer from N12 back to O14 to yield a closed-shell species that relaxes to the S_0 equilibrium structure S0-MIN (Figure 9). Population analysis shows that it is a hydrogen and not a proton which migrates during the rearrangement. According to the OM2/MRCI dynamics simulations, this reverse hydrogen transfer is also quite fast in vacuum and occurs typically after around 450 fs.

Thereafter, the molecule moves toward the ground-state minimum (S0-MIN). On the way, it acquires much kinetic energy by converting the electronic energy available after the $S_1(^1\pi\pi^*) \rightarrow S_0$ radiationless transition. This accumulated kinetic energy is sufficient to overcome the S_0 barrier for rotation around the C6–C7 bond (Figure 4). The corresponding transition state (S0-TS) has been optimized at the B3LYP/6-31+G* level, and its geometric parameters are listed in Table

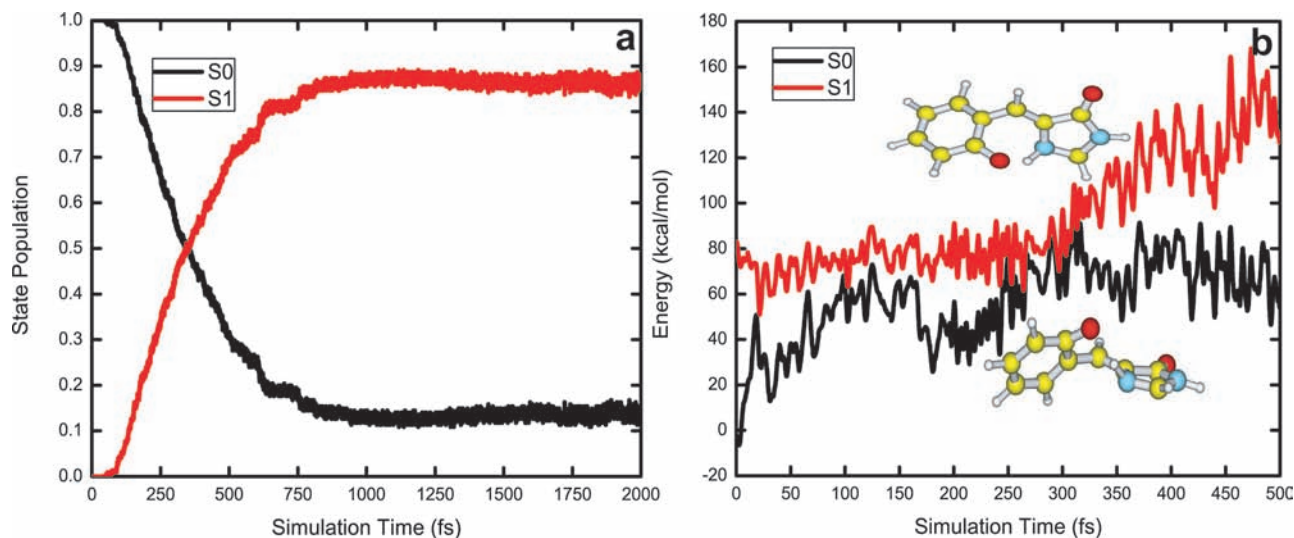


Figure 8. Time-dependent S_1 and S_0 state populations (panel a) during 2000 fs nonadiabatic simulations (OM2/MRCI) and time-dependent potential energies (panel b) of S_1 and S_0 states from a typical trajectory.

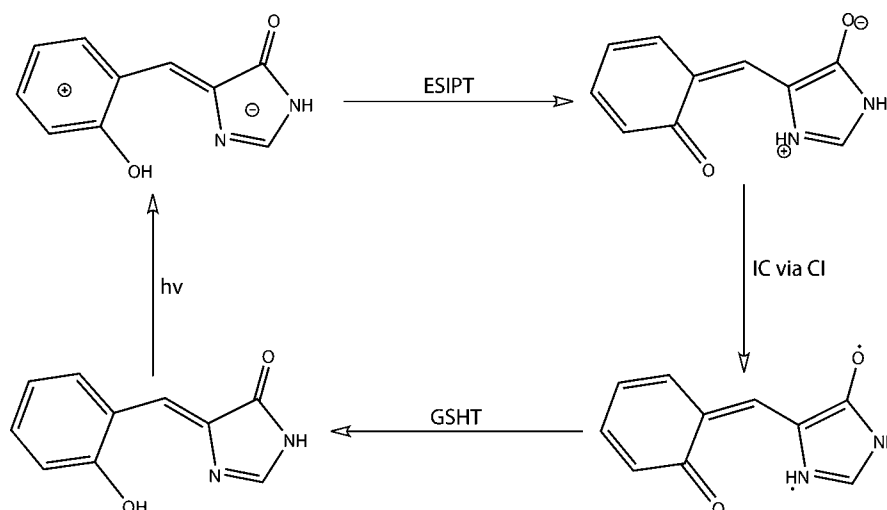


Figure 9. Charge-transfer induced excited-state intramolecular proton transfer (ESIPT), internal conversion (IC) via conical intersection (CI), and ground-state hydrogen transfer (GSHT).

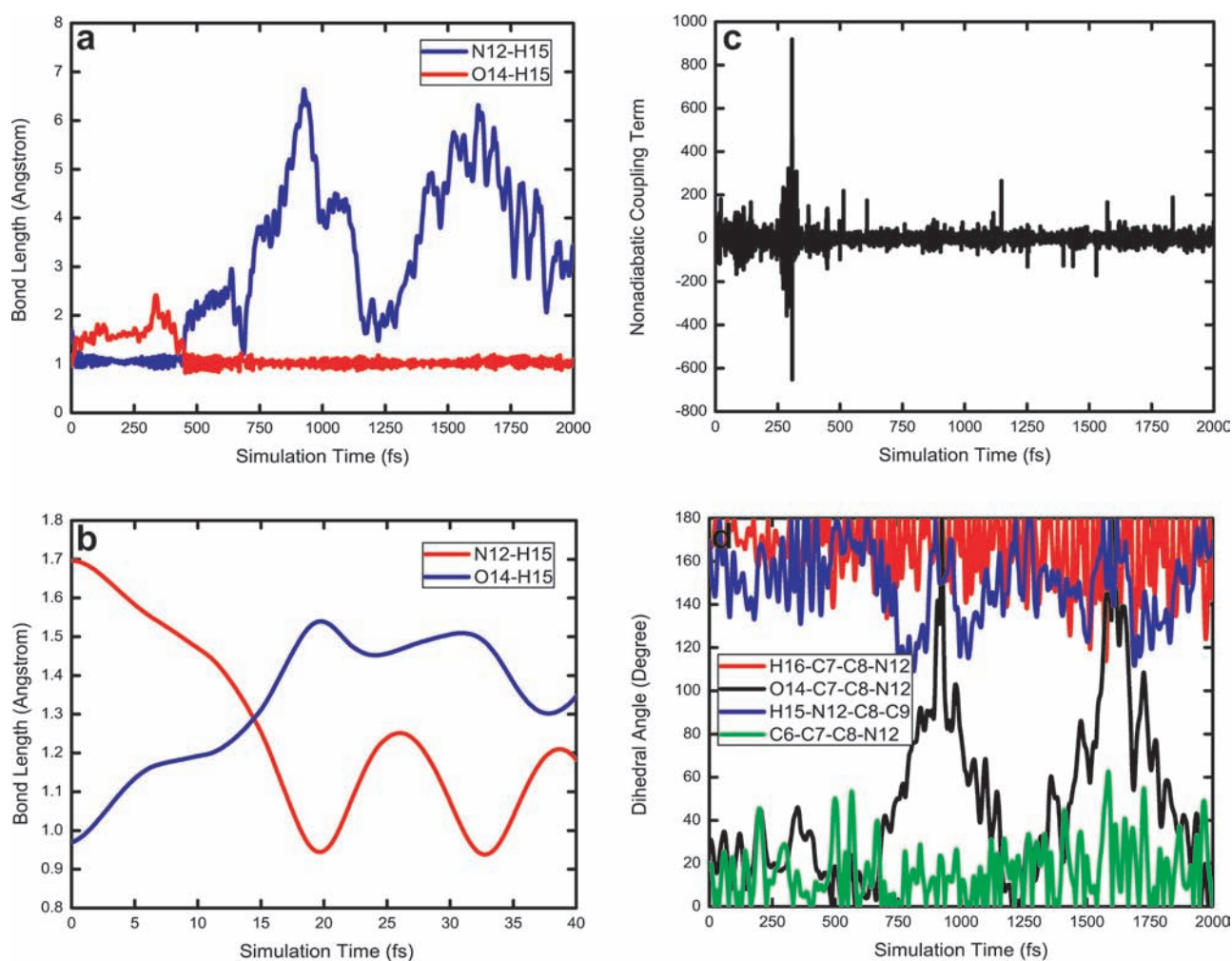


Figure 10. Time-dependent physical variables from a typical OM2/MRCI trajectory. (Panel a) N12–H15 and O1–H15 distances over the whole simulation time of 2000 fs; (panel b) N12–H15 and O1–H15 distances during the first 40 fs; (panel c) nonadiabatic coupling term; (panel d) time evolution of four key dihedral angles.

1. The rotational barrier is predicted to be 15.7 kcal/mol (B3LYP/6-31+G*). It can easily be crossed by the “hot” OHBI molecule; hence, such rotational motion around the C6–C7 bond repeatedly takes place in the OM2/MRCI surface-

hopping dynamics simulations after the reverse hydrogen transfer is finished.

A Typical Trajectory. A typical trajectory is shown in Figure 10. In this particular case, the $S_1(^1\pi\pi^*)$ state of OHBI

decays to the S_0 state at around 300 fs, when the $S_1(^1\pi\pi^*)$ and S_0 states come close to each other energetically (see panel b of Figure 8) and strongly interact through a large nonadiabatic coupling term (see panel c of Figure 10). Upon photoexcitation, the O14–H15 bond dissociates within about 20 fs (panel b of Figure 10); thereafter, the O14–H15 distance oscillates around 1.5–2.0 Å, first in the S_1 state and then—after the internal conversion at about 300 fs—in the S_0 state, until the ground-state hydrogen transfer from N12 back to O14 occurs at about 450 fs (see panel a of Figure 10). Conversely, the N12–H15 distance decreases within the first 20 fs from initially about 1.7 Å to about 1 Å; after the ground-state hydrogen transfer, it adopts much larger values that show periodic fluctuations due to the internal rotation around the C6–C7 bond, which is rather facile in the S_0 state (see above). The time evolution of the O14–C7–C8–N12 dihedral angle (see panel d of Figure 10) illustrates this twisting motion of the two rings: two cycles of rotation are observed, with turning points around 900 and 1600 fs. One should note, however, that this internal rotation could possibly be blocked in solution because of the cage effect of the solvent (which is not considered presently).

In our trajectory calculations, we have not considered the effect of replacing hydrogen by deuterium in the intramolecular hydrogen bond. Since the initial proton transfer in the S_1 state is barrierless, there is no tunneling during the ESIPT process, and the H/D replacement should thus only have a minor effect on the dynamics. This is consistent with the reported lack of deuterium isotope dependence in the rise dynamics.⁶¹

Photophysical and Photochemical Mechanisms. The static electronic structure calculations and the nonadiabatic dynamics simulations yield the following overall scenario for the photoinduced processes in OHBI (Figure 11). First, a photon excites OHBI to the $S_1(^1\pi\pi^*)$ state in the Franck–Condon region which is accompanied by some intramolecular

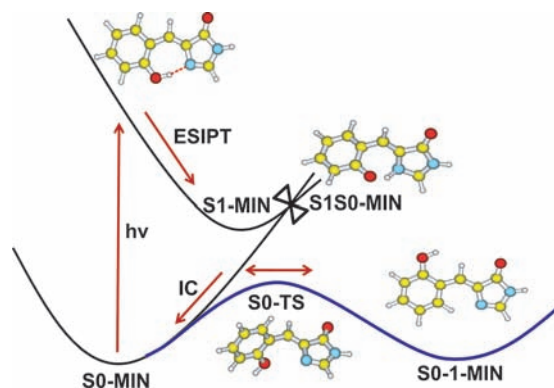
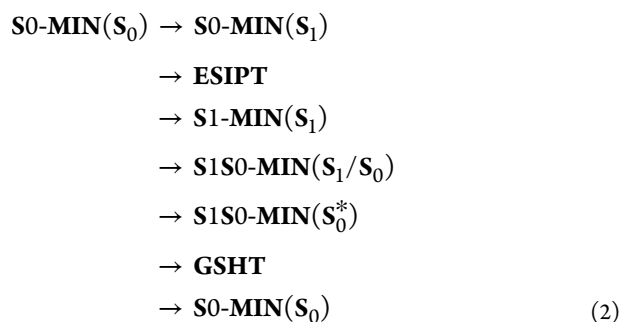


Figure 11. Photoinduced decay mechanism suggested by the present electronic structure calculations and nonadiabatic dynamics simulations. The black and blue lines mainly involve the proton transfer coordinate (O14–H15) and single-bond rotation coordinate (C1–C6–C7–C8), respectively.

charge transfer from the six- to the five-membered ring (Figure 5); second, an excited-state intramolecular proton transfer (ESIPT) takes place (Figure 9) that rapidly leads to the $S_1(^1\pi\pi^*)$ minimum-energy structure, S1-MIN; third, near S1-MIN, the $S_1(^1\pi\pi^*)/S_0$ minimum-energy conical intersection S1S0-MIN funnels the $S_1(^1\pi\pi^*)$ electronic population to the S_0 state, and the excess electronic energy is converted into S_0

internal energy; fourth, a ground-state reverse hydrogen transfer (GSHT)—with the H15 atom moving back from N12 to O15—takes place, forming S0-MIN; finally, the excess kinetic energy leads to rotational motion around the C6–C7 single bond. This mechanism can be summarized as follows:



Concerning the first two stages of this mechanism, one should emphasize that the ESIPT process is induced by the charge transfer originating from the $S_0 \rightarrow S_1(^1\pi\pi^*)$ electronic transition in the Franck–Condon region. This kind of charge-transfer induced proton transfer has previously been seen in a number of other systems, including nucleobase pairs.^{96–102}

Our proposed mechanism is consistent with the experimental observation of dominant ultrafast excited-state intramolecular proton transfer and subsequent $S_1 \rightarrow S_0$ internal conversion in OHBDI.⁶¹ Furthermore, in the OM2/MRCI 2-ps nonadiabatic simulations, no cis–trans isomerization event is observed in the $S_1(^1\pi\pi^*)$ state, which is not unexpected, given the experimental finding that the yield of cis–trans isomerization in OHBDI is less than 5% in various solvents.⁶¹ Experimental information on the ground-state hydrogen transfer is available only for the trans-isomer of OHBDI in solution (i.e., for the minor branch not seen in our simulation), where it occurs by a rather slow two-step process of deprotonation and proton recombination on the microsecond time scale.⁶¹

It is instructive to compare the photophysical and photochemical mechanisms of OHBI and PHBI. Mechanistic discrepancies usually root in different geometric and electronic structures. Geometrically, the most remarkable difference is the position of the OH group at the six-membered ring—ortho in OHBI and para in PHBI (Figure 2). It is thus possible for OHBI to form an intramolecular hydrogen bond, but not for PHBI, which can at best engage in intermolecular hydrogen bonding in solution or in proteins where nearby solvent molecules or residues may serve as a bridge connecting the donor and acceptor atoms. Experimentally, the excited state intramolecular proton transfer takes place rapidly within tens of femtoseconds in OHBDI,⁶¹ while this process is not observed at all in PHBDI.¹⁵ The reverse hydrogen transfer that occurs in OHBI after the radiationless return to the ground state, is also a result of the intramolecular hydrogen bonding. This structural feature thus governs both the excited-state and ground-state dynamics of OHBI after photoexcitation.

The presence or absence of the intramolecular hydrogen bond also determines the character of the $S_1(^1\pi\pi^*)/S_0$ minimum-energy conical intersections, and hence the decay mechanisms, in OHBI and PHBI. In the absence of this hydrogen bond, the two rings are nearly perpendicular to each other at the $S_1(^1\pi\pi^*)/S_0$ minimum-energy conical intersection in PHBI;^{15,27,39,41,42,48} since the twisted C7–C8 double bond nearly approaches 90° at this intersection, PHBI can bifurcate into the cis and trans isomers when it reaches this funnel point.

By contrast, in OHBI, the C7–C8 bond is only slightly twisted at the $S_1(^1\pi\pi^*)/S_0$ minimum-energy conical intersection (S1S0-MIN, dihedral angle of -11.7° , see Table 1), and hence, the overwhelming majority of trajectories will retain the cis conformation during internal conversion and also during the subsequent ground-state reverse hydrogen transfer; consequently, no cis–trans isomerization is observed in the OM2/MRCI dynamics simulations of OHBI (experimentally, less than 5% in OHBDI). The intramolecular hydrogen-bonding interaction thus has a crucial influence not only on the photophysical and photochemical mechanisms but also on the yield of the cis–trans isomerization.

Relation to Previous Experimental Work. The overall mechanism derived from recent spectroscopic work on OHBDI⁶¹ is compatible with the present computational results for OHBI with regard to its general features. The key advantage of our current calculations is that they provide a detailed microscopic understanding of the photoinduced processes and thus go beyond of what can be deduced from experiment alone. This includes the characterization of the electronic structure of all relevant species, the prediction of their properties (e.g., structures, energies, dipole moments, lifetimes), and the direct simulation of the nonadiabatic dynamics after photoexcitation. In the following, we briefly address three topics where the present work provides new qualitative insights.

First, the $S_0 \rightarrow S_1$ transition is accompanied by charge transfer, with a substantial amount of negative charge being shifted from the phenyl to the imidazole ring. This induces the subsequent excited-state intramolecular proton transfer that happens very quickly (on the fs scale) to adapt to the electronic polarization created upon photoexcitation. The dynamics simulations provide a detailed mechanistic scenario for this charge-transfer-induced excited-state proton transfer in OHBI, which is specific for the ortho-substituted GFP chromophore and does not occur in para-substituted counterparts such as PHBI. This kind of coupled electron–proton transfer has been found in other systems, e.g., in DNA base pairs,^{96–99,101,102} but is now identified and characterized for the first time in GFP-type chromophores.

Second, the experimentally observed quantum yield of cis–trans isomerization is very low for OHBI (less than 5%)⁶¹ and quite high for PHBI in solution.^{21,50,53} Our calculations allow us to understand the origin of this discrepancy, in terms of the conical intersection that mediates the $S_1 \rightarrow S_0$ internal conversion in OHBI and PHBI. We find that the conical intersection structure in OHBI (S1S0-MIN) contains an intramolecular hydrogen-bonding interaction connecting the two rings of OHBI, which constrains the geometry to remain close to planar (i.e., close to the cis conformer), and strongly favors the return to the cis form after the $S_1 \rightarrow S_0$ internal conversion. By contrast, in the conical intersection structure of PHBI, the two rings are nearly perpendicular to each other, and hence the system can proceed almost equally well to the cis or trans form after the internal conversion. Our scenario for OHBI differs from the suggestion⁶¹ that it is the rotation of the exocyclic C7=C8 double bond which triggers a fast $S_1 \rightarrow S_0$ internal conversion process.

Third, it has been unclear up to now whether the trans conformer of OHBI (5% yield) is formed by an excited-state or a ground-state process. Our present simulations show that the $S_1 \rightarrow S_0$ internal conversion is ultrafast in OHBI and proceeds via a nearly planar conical intersection (S1S0-MIN); hence, the central double-bond isomerization cannot occur in the excited

state. We thus conclude that the trans conformer is produced by a ground-state isomerization, which is known to involve a large barrier (consistent with the low yield of 5%).

CONCLUSION AND OUTLOOK

OHBDI is a recently synthesized GFP chromophore.⁶⁰ It exhibits unusual photophysical and photochemical behavior that is totally different from that of previously available synthetic analogues of the GFP core chromophore, such as PHBDI.⁶¹ To understand these differences, we have optimized the crucial points on the S_0 and $S_1(^1\pi\pi^*)$ potential energy surfaces of OHBI (minima, transition state, and conical intersection) using ab initio, DFT, and semiempirical methods, and have carried out OM2/MRCI nonadiabatic surface-hopping simulations to study the actual photodynamics. The present results are consistent with the experimental findings for OHBDI and rationalize several key observations, namely the very low yield of cis–trans isomerization, the ultrafast excited-state intramolecular proton transfer, and the ground-state reverse hydrogen transfer.⁶¹ The differences in the photoinduced processes of OHBI and PHBI are attributed to the presence or absence of the crucial intramolecular hydrogen-bonding interaction between the two rings.

According to our present calculations, the nonadiabatic decay of OHBI in the gas phase occurs on the fs time scale and is thus intrinsically fast. Experimentally, it would be desirable to further examine this predicted gas-phase behavior by ultrafast pump–probe and femtosecond Raman techniques.^{103–105} In view of the computed intrinsic properties of OHBI, the prospects of using such 2-hydroxy-substituted GFP chromophores as fluorescence markers in biological systems would appear to be rather dim. The measured fluorescence quantum yields of OHBDI-based chromophores are indeed extremely low in aprotic solvents, e.g., 1.5×10^{-3} in CH_3CN .⁶¹ On the other hand, much higher fluorescence quantum yields (up to 0.4) have been observed when OHBDI is placed into a solid film,⁶⁰ and experimentalists have expressed their belief that it may be possible to tune fluorescence emission and to slow down internal conversion by chemically tailoring such chromophores.^{60,62} In the complex environment of a protein, distinct hydrogen-bonding interactions with surrounding residues, anisotropic electrostatic interactions, and steric interactions may affect the accessibility to conical intersections and hence the time scale of internal conversion, or may even alter the course of the photophysical and photochemical events.¹⁰⁶ The protein environment may thus block fast internal conversion processes that exist in the gas phase, as proposed for other photoreceptor systems.¹⁰⁶ Given this situation, it seems worthwhile to investigate the photoinduced processes of OHBI-type chromophores incorporated into various GFPs, both experimentally and theoretically.

ASSOCIATED CONTENT

Supporting Information

Cartesian coordinates of all optimized structures and complete reference 78. This material is available free of charge via the Internet at <http://pubs.acs.org>.

AUTHOR INFORMATION

Corresponding Author

thiel@mpi-muelheim.mpg.de

REFERENCES

- (1) Chalfie, M.; Tu, Y.; Euskirchen, G.; Ward, W. W.; Prasher, D. C. *Science* **1994**, *263*, 802.
- (2) Tsien, R. *Annu. Rev. Biochem.* **1998**, *67*, 509.
- (3) Chatteraj, M.; King, B. A.; Bublitz, G. U.; Boxer, S. G. *Proc. Natl. Acad. Sci. U.S.A.* **1996**, *93*, 8362.
- (4) Lill, M. A.; Helms, V. *Proc. Natl. Acad. Sci. U.S.A.* **2002**, *99*, 2778.
- (5) Patterson, G. H.; Lippincott-Schwartz, J. *Science* **2002**, *297*, 1873.
- (6) Lippincott-Schwartz, J.; Patterson, G. H. *Science* **2003**, *300*, 87.
- (7) Meech, S. *Chem. Soc. Rev.* **2009**, *38*, 2922.
- (8) Zimmer, M. *Chem. Rev.* **2002**, *102*, 759.
- (9) Nienhaus, G. U. *Angew. Chem., Int. Ed.* **2008**, *47*, 8992.
- (10) Fang, C.; Frontiera, R. R.; Tran, R.; Mathies, R. A. *Nature* **2009**, *462*, 200.
- (11) Tonge, P. J.; Meech, S. R. *J. Photochem. Photobiol. A: Chem.* **2009**, *205*, 1.
- (12) van Thor, J. J.; Gensch, T.; Hellingwerf, K. J.; Johnson, L. N. *Nat. Struct. Biol.* **2002**, *9*, 37.
- (13) Toniolo, A.; Granucci, G.; Martinez, T. J. *J. Phys. Chem. A* **2003**, *107*, 3822.
- (14) Megley, C. M.; Dickson, L. A.; Maddalo, S. L.; Chandler, G. J.; Zimmer, M. *J. Phys. Chem. B* **2009**, *113*, 302.
- (15) Toniolo, A.; Olsen, S.; Manohar, L.; Martinez, T. J. *Faraday Discuss.* **2004**, *127*, 149.
- (16) Martin, M. E.; Negri, F.; Olivucci, M. *J. Am. Chem. Soc.* **2004**, *126*, 5452.
- (17) Altoe, P.; Bernardi, F.; Garavelli, M.; Orlandi, G.; Negri, F. *J. Am. Chem. Soc.* **2005**, *127*, 3952.
- (18) Henderson, J. N.; Osborn, M. F.; Koon, N.; Gepshtein, R.; Huppert, D.; Remington, S. J. *J. Am. Chem. Soc.* **2009**, *131*, 13212.
- (19) Henderson, J. N.; Gepshtein, R.; Heenan, J. R.; Kallio, K.; Huppert, D.; Remington, S. J. *J. Am. Chem. Soc.* **2009**, *131*, 4176.
- (20) Kondo, M.; Heisler, I. A.; Stoner-Ma, D.; Tonge, P. J.; Meech, S. R. *J. Am. Chem. Soc.* **2010**, *132*, 1452.
- (21) Mudalige, K.; Habuchi, S.; Goodwin, P. M.; Pai, R. K.; De Schryver, F.; Cotlet, M. *J. Phys. Chem. B* **2010**, *114*, 4678.
- (22) Stoner-Ma, D.; Jaye, A. A.; Ronayne, K. L.; Nappa, J.; Meech, S. R.; Tonge, P. J. *J. Am. Chem. Soc.* **2008**, *130*, 1227.
- (23) Sinicropi, A.; Andruniow, T.; Ferre, N.; Basosi, R.; Olivucci, M. *J. Am. Chem. Soc.* **2005**, *127*, 11534.
- (24) Voityuk, A. A.; Michel-Beyerle, M. E.; Rösch, N. *Chem. Phys. Lett.* **1997**, *272*, 162.
- (25) Weber, W.; Helms, V.; McCammon, J. A.; Langhoff, P. W. *Proc. Natl. Acad. Sci. U.S.A.* **1999**, *96*, 6177.
- (26) Gross, L. A.; Baird, G. S.; Hoffman, R. C.; Baldrige, K. K.; Tsien, R. Y. *Proc. Natl. Acad. Sci. U.S.A.* **2000**, *97*, 11990.
- (27) Schäfer, L. V.; Groenhof, G.; Klingen, A. R.; Ullmann, G. M.; Boggio-Pasqua, M.; Robb, M. A.; Grubmüller, H. *Angew. Chem., Int. Ed.* **2007**, *46*, 530.
- (28) Wan, S.; Liu, S.; Zhao, G.; Chen, M.; Han, K.; Sun, M. *Biophys. Chem.* **2007**, *129*, 218.
- (29) Topol, I.; Collins, J.; Polyakov, I.; Grigorenko, B.; Nemukhin, A. *Biophys. Chem.* **2009**, *145*, 1.
- (30) Marques, M. A. L.; Lopez, X.; Varsano, D.; Castro, A.; Rubio, A. *Phys. Rev. B Lett.* **2003**, *90*, 258101.
- (31) Lopez, X.; Marques, M. A. L.; Castro, A.; Rubio, A. *J. Am. Chem. Soc.* **2005**, *127*, 12329.
- (32) Xie, D.; Zeng, X. *J. Comput. Chem.* **2005**, *26*, 1487.
- (33) Nemukhin, A. V.; Topol, I. A.; Burt, S. K. *J. Chem. Theory Comput.* **2006**, *2*, 292.
- (34) Sun, M. *Int. J. Quantum Chem.* **2006**, *106*, 1020.
- (35) Amat, P.; Granucci, G.; Buda, F.; Persico, M.; Tozzini, V. *J. Phys. Chem. B* **2006**, *110*, 9348.
- (36) Timerghazin, Q. K.; Carlson, H. J.; Liang, C.; Campbell, R. E.; Brown, A. J. *J. Phys. Chem. B* **2008**, *112*, 2533.
- (37) Helms, V.; Winstead, C.; Langhoff, P. W. *THEOCHEM* **2000**, *506*, 179.
- (38) Das, A. K.; Hasegawa, J.-Y.; Miyahara, T.; Ehara, M.; Nakatsuji, H. *J. Comput. Chem.* **2003**, *24*, 1421.
- (39) Olsen, S.; Smith, S. C. *J. Am. Chem. Soc.* **2007**, *129*, 2054.
- (40) Bravaya, K. B.; Bochenkova, A. V.; Granovsky, A. A.; Savitsky, A. P.; Nemukhin, A. V. *J. Phys. Chem. A* **2008**, *112*, 8804.
- (41) Olsen, S.; Smith, S. C. *J. Am. Chem. Soc.* **2008**, *130*, 8677.
- (42) Virshup, A. M.; Punwong, C.; Pogorelov, T. V.; Lindquist, B. A.; Ko, C.; Martinez, T. J. *J. Phys. Chem. B* **2009**, *113*, 3280.
- (43) Epifanovsky, E.; Polyakov, I.; Grigorenko, B.; Nemukhin, A.; Krylov, A. I. *J. Chem. Theory Comput.* **2009**, *5*, 1895.
- (44) Polyakov, I.; Epifanovsky, E.; Grigorenko, B.; Krylov, A. I.; Nemukhin, A. *J. Chem. Theory Comput.* **2009**, *5*, 1907.
- (45) Polyakov, I. V.; Grigorenko, B. L.; Epifanovsky, E. M.; Krylov, A. I.; Nemukhin, A. V. *J. Chem. Theory Comput.* **2010**, *6*, 2377.
- (46) Filippi, C.; Zaccheddu, M.; Buda, F. *J. Chem. Theory Comput.* **2009**, *5*, 2047.
- (47) Ma, Y.; Rohlfing, M.; Molteni, C. *J. Chem. Theory Comput.* **2010**, *6*, 257.
- (48) Olsen, S.; Lamothe, K.; Martinez, T. J. *J. Am. Chem. Soc.* **2010**, *132*, 1192.
- (49) Usman, A.; Mohammed, O. F.; Nibbering, E. T. J.; Dong, J.; Solntsev, K. M.; Tolbert, L. M. *J. Am. Chem. Soc.* **2005**, *127*, 11214.
- (50) Forbes, M. W.; Jockusch, R. A. *J. Am. Chem. Soc.* **2009**, *132*, 17038.
- (51) Rajput, J.; Rahbek, D. B.; Andersen, L. H.; Rocha-Rinza, T.; Christiansen, O.; Bravaya, K. B.; Erokhin, A. V.; Bochenkova, A. V.; Solntsev, K. M.; Dong, J.; Kowalik, J.; Tolbert, L. M.; Petersen, M. A.; Nielsen, M. B. *Phys. Chem. Chem. Phys.* **2009**, *11*, 9996.
- (52) Schäfer, L. V.; Groenhof, G.; Boggio-Pasqua, M.; Robb, M. A.; Grubmüller, H. *PLoS Comput. Biol.* **2008**, *4*, e1000034.
- (53) Stavrov, S. S.; Solntsev, K. M.; Tolbert, L. M.; Huppert, D. *J. Am. Chem. Soc.* **2006**, *128*, 1540.
- (54) Altun, A.; Yokoyama, S.; Morokuma, K. *J. Phys. Chem. B* **2008**, *112*, 16883.
- (55) Boggio-Pasqua, M.; Robb, M. A.; Groenhof, G. *J. Am. Chem. Soc.* **2009**, *131*, 13580.
- (56) Li, X.; Chung, L.; Mizuno, H.; Miyawaki, A.; Morokuma, K. *J. Phys. Chem. B* **2009**, *114*, 1114.
- (57) Li, X.; Chung, L.; Mizuno, H.; Miyawaki, A.; Morokuma, K. *J. Phys. Chem. B* **2010**, *114*, 16666.
- (58) Li, X.; Chung, L.; Mizuno, H.; Miyawaki, A.; Morokuma, K. *J. Phys. Chem. Lett.* **2010**, *1*, 3328.
- (59) Sekharan, S.; Morokuma, K. *J. Am. Chem. Soc.* **2011**, *133*, 4734.
- (60) Chen, K. Y.; Cheng, Y. M.; Lai, C. H.; Hsu, C. C.; Ho, M. L.; Lee, G. H.; Chou, P. T. *J. Am. Chem. Soc.* **2007**, *129*, 4534.
- (61) Hsieh, C. C.; Chou, P. T.; Shih, C. W.; Chuang, W. T.; Chung, M. W.; Lee, J. H.; Joo, T. H. *J. Am. Chem. Soc.* **2011**, *133*, 2932.
- (62) Conyard, J.; Kondo, M.; Heisler, I. A.; Jones, G.; Baldrige, A.; Tolbert, L. M.; Solntsev, K. M.; Meech, S. R. *J. Phys. Chem. B* **2011**, *115*, 1571.
- (63) Parr, R. G.; Yang, W. T. *Density-Functional Theory of Atoms and Molecules*; Oxford University Press: New York, 1994.
- (64) Christiansen, O.; Koch, H.; Jorgensen, P. *Chem. Phys. Lett.* **1995**, *243*, 409.
- (65) Hättig, C.; Weigend, F. *J. Chem. Phys.* **2000**, *113*, 5154.
- (66) Hättig, C.; Köhn, A. *J. Chem. Phys.* **2002**, *117*, 6939.
- (67) *Time-dependent Density Functional*; Marques, M. A. L., Ullrich, C. A., Nogueira, F., Rubio, A., Burke, K., Gross, E. K. U., Eds.; Springer: New York, 2006.
- (68) Lee, C. T.; Yang, W. T.; Parr, R. G. *Phys. Rev. B* **1988**, *37*, 785.
- (69) Becke, A. D. *J. Chem. Phys.* **1993**, *98*, 5648.
- (70) Grimme, S.; Waletzke, M. *J. Chem. Phys.* **1999**, *111*, 5645.
- (71) Yanai, T.; Tew, D. P.; Handy, N. C. *Chem. Phys. Lett.* **2004**, *393*, 51.
- (72) Chai, J. D.; Head-Gordon, M. *J. Chem. Phys.* **2008**, *128*, 084106.
- (73) Zhao, Y.; Truhlar, D. G. *Theor. Chem. Acc.* **2008**, *120*, 215.
- (74) Becke, A. D. *J. Chem. Phys.* **1993**, *98*, 1372.
- (75) Ditchfield, R.; Hehre, W. J.; Pople, J. A. *J. Chem. Phys.* **1971**, *54*, 724.
- (76) Dunning, T. H. Jr. *J. Chem. Phys.* **1989**, *90*, 1007.

- (77) Schäfer, A.; Huber, C.; Ahlrichs, R. *J. Chem. Phys.* **1994**, *100*, 5829.
- (78) Frisch, M. J.; et al. *Gaussian 09*, Revision A.02; Gaussian, Inc.: Wallingford, CT, 2009.
- (79) Ahlrichs, R.; Bär, M.; Häser, M.; Horn, H.; Kölmel, C. *Chem. Phys. Lett.* **1989**, *162*, 165.
- (80) Weber, W. Ph.D. Thesis, University of Zürich, 1996.
- (81) Weber, W.; Thiel, W. *Theor. Chem. Acc.* **2000**, *103*, 495.
- (82) Koslowski, A.; Beck, M. E.; Thiel, W. *J. Comput. Chem.* **2003**, *24*, 714.
- (83) Silva-Junior, M. R.; Thiel, W. *J. Chem. Theory Comput.* **2010**, *6*, 1546.
- (84) Thiel, W. *MNDO99 Program*, version 6.1; Max-Planck-Institut für Kohlenforschung: Mülheim, Germany, 2007.
- (85) Keal, T. W.; Wanko, M.; Thiel, W. *Theor. Chem. Acc.* **2009**, *123*, 145.
- (86) Fabiano, E.; Keal, T. W.; Thiel, W. *Chem. Phys.* **2008**, *349*, 334.
- (87) Fabiano, E.; Thiel, W. *J. Phys. Chem. A* **2008**, *112*, 6859.
- (88) Tully, J. C.; Preston, R. K. *J. Chem. Phys.* **1971**, *55*, 562.
- (89) Hammes-Schiffer, S.; Tully, J. C. *J. Chem. Phys.* **1994**, *101*, 4657.
- (90) Cui, G. L.; Ai, Y. J.; Fang, W. H. *J. Phys. Chem. A* **2010**, *114*, 730.
- (91) Lan, Z. G.; Fabiano, E.; Thiel, W. *ChemPhysChem* **2009**, *10*, 1225.
- (92) Lan, Z. G.; Fabiano, E.; Thiel, W. *J. Phys. Chem. B* **2009**, *113*, 3548.
- (93) Weingart, O.; Lan, Z.; Koslowski, A.; Thiel, W. *J. Phys. Chem. Lett.* **2011**, *2*, 1506.
- (94) Kazaryan, A.; Lan, Z.; Schäfer, L. V.; Thiel, W.; Filatov, M. *J. Chem. Theory Comput.* **2011**, *7*, 2189.
- (95) Lan, Z.; Lu, Y.; Fabiano, E.; Thiel, W. *ChemPhysChem* **2011**, *12*, 1989.
- (96) Doltsinis, N. *Mol. Phys.* **2004**, *102*, 499.
- (97) Coe, J.; Martnez, T. *J. Am. Chem. Soc.* **2005**, *127*, 4560.
- (98) Sobolewski, A. L.; Domcke, W.; Hättig, C. *Proc. Natl. Acad. Sci. U.S.A.* **2005**, *102*, 17903.
- (99) Perun, S.; Sobolewski, A. L.; Domcke, W. *J. Phys. Chem. A* **2006**, *110*, 9031.
- (100) Groenhof, G.; Schäfer, L. V.; Boggio-Pasqua, M.; Goette, M.; Grubmüller, H.; Robb, M. A. *J. Am. Chem. Soc.* **2007**, *129*, 6812.
- (101) Markwick, P. R. L.; Doltsinis, N. L. *J. Chem. Phys.* **2007**, *126*, 175102.
- (102) Ai, Y. J.; Zhang, F.; Cui, G. L.; Luo, Y.; Fang, W. H. *J. Chem. Phys.* **2010**, *133*, 064302.
- (103) Kukura, P.; McCamant, D. W.; Yoon, S.; Wandschneider, D. B.; Mathies, R. A. *Science* **2005**, *310*, 1006.
- (104) Fang, C.; Frontiera, R.; Tran, R.; Mathies, R. *Nature* **2009**, *462*, 200.
- (105) Polli, D.; Altoè, P.; Weingart, O.; Spillane, K. M.; Manzoni, C.; Brida, D.; Tomasello, G.; Orlandi, G.; Kukura, P.; Mathies, R. A.; Garavelli, M.; Cerullo, G. *Nature* **2010**, *467*, 440.
- (106) Merz, T.; Sadeghian, K.; Schütz, M. *Phys. Chem. Chem. Phys.* **2011**, *13*, 14775.